THE ASTROPHYSICAL JOURNAL, 463:134–143, 1996 May 20

COMPLEX ABSORPTION IN THE SEYFERT 1 GALAXY ESO 055620−3820.2

T. J. TURNER,[1,2] H. NETZER,[3] AND I. M. GEORGE[1,2]
Received 1995 August 22; accepted 1995 November 16

ABSTRACT

We report the results from an *ASCA* observation which yields the first contaminated hard X-ray spectrum of the Seyfert 1 galaxy EXO 055620−3820.2. We find the source spectrum to exhibit a complex structure below 2 keV, indicating that the continuum is attenuated either by an ionized absorber fully or partially covering the X-ray source, or a neutral absorber partially covering the source. While the X-ray data alone do not allow us to distinguish between these models, consideration of the optical properties of this highly reddened nucleus suggests that partial covering by neutral material is unlikely, as it implies an unusually large intrinsic optical flux. We find a good fit to the X-ray data, and consistency with the observed optical properties of the source, with either 96% of the source covered by a column of 3.1×10^{22} cm^{-2} of low-ionization gas or full covering by a column of 3.6×10^{22} cm^{-2} of highly ionized gas. Both models required extinction of the optical continuum by dust in the host galaxy with $A_V \sim 2$ mag. We find evidence for a column of neutral material associated with this dust. The partial-covering models leave a residual soft excess below 1 keV, and the possible origin of this soft emission is also discussed.

We detect an iron *K*-shell emission line, which appears to be significantly broad, with an equivalent width (∼300 eV) exceeding that predicted from the absorbing material along the line of sight. The line is consistent with emission from neutral iron, and we find a FWHM for the line of 31,000–77,000 km s^{-1}, similar to several other Seyfert spectra reported recently.

Subject headings: galaxies: individual: EXO 055620−3820.2 — galaxies: Seyfert — X-rays: galaxies

1. INTRODUCTION

Observations over the last few years have shown that many active galactic nuclei (AGNs) contain significant amounts of circumnuclear material which reprocesses and hence substantially modifies the intrinsic X-ray radiation. Partially ionized X-ray absorbers were first suggested to exist close to AGNs when flux-correlated spectral variability was observed in sources such as MR 2251−178 (Halpern 1984; Pan, Stewart, & Pounds 1990) and NGC 4151 (Fiore, Perola, & Ramano 1990; Yaqoob & Warwick 1991). Supporting evidence for such so-called warm absorbers was later provided by *Ginga* observations of emission-line AGNs which revealed iron K-shell features in some sources, suggestive of an origin in ionized material (e.g., Nandra & Pounds 1994). Additional observational support for the existence of warm absorbers came from *ROSAT* Position Sensitive Proportional Counter (PSPC) observations, which clearly showed a deficit of photons close to ∼0.8 keV, interpreted as absorption by ionized oxygen in sources such as MCG−6-30-15 (Nandra & Pounds 1992), 3C 351 (Fiore et al. 1993), and NGC 3783 (Turner et al. 1993). These results are confirmed by *ASCA* observations (e.g., Fabian et al. 1994; George, Turner, & Netzer 1995; Reynolds et al. 1995a). Ionized absorbers are now thought to be common among low-luminosity AGNs. Indeed, Nandra & Pounds (1994) find that 12 out of 27 sources in their sample (Seyfert 1 galaxies and narrow emission line galaxies [NELGS]) show some evidence for such a component.

Theoretical work on such ionized gas has been presented by several workers, including Halpern (1984), Krolik & Kallman (1984), Ferland & Rees (1988), Yaqoob (1990), Netzer (1993), Marthur et al. (1994), Reynolds & Fabian (1995), and Krolik & Kriss (1995). While the physics of the ionized gas is thought to be well understood (Netzer 1993), severe difficulties are encountered in modeling the observed spectral features. In particular, combined variability and spectral analysis suggest the assumption of a single ionized component along the line of sight may be somewhat simplistic (e.g., Fabian et al. 1994; Reynolds et al. 1995a). The geometry of the innermost regions of AGNs are probably highly complex, and the number of X-ray spectral features currently observable is not large enough to constrain all possible models.

The hard X-ray source 3A0557−383, also detected in the *HEAO 1* A-2 (H0557-385) and *Uhuru* (*4U* 0557−38) surveys, was originally identified with a Seyfert 1 galaxy of redshift $z = 0.03440$ (Fairall, McHardy, & Pye 1982), and included in the hard X-ray log *N*–log *S* and luminosity function of Seyfert galaxies (Piccinotti et al. 1982). However, a subsequent study by Giommi et al. (1989), using the *EXOSAT* channel multiplier array (CMA) instrument, revealed two X-ray–emitting AGNs within ∼25′ of each other: the BL Lac object, EX 055625−3838.6 with an optical position (J2000) $05^h58^m05^s.3$, $-38°38'23''.9$, and the Seyfert 1 galaxy EXO 055620−3820.2 with an optical position (J2000) $05^h58^m02^s.0$, $-38°20'04''.7$. The hard X-ray source previously observed by passively collimated detectors may have had contributions from both the Seyfert and BL Lac. However, separation is large enough so that confusion between the two sources is not a problem for *ASCA*. Here we present the first uncontaminated hard X-ray spectrum of EXO 055620−3820.2. The results from the BL Lac object EXO 055625−3838.6 are presented elsewhere (George & Turner 1996).

[1] Laboratory for High Energy Astrophysics, Code 660.2, NASA/Goddard Space Flight Center, Greenbelt, MD 20771.
[2] Universities Space Research Association.
[3] School of Physics and Astronomy and Wise Observatory, Beverly and Raymond Sackler Faculty of Exact Sciences, Tel Aviv University, Tel Aviv 69978, Israel.

In § 2 below we present new *ASCA* observations of EXO 055620−3820.2, and in § 3 we describe several complex models we have used to fit the X-ray data. The discussion in § 4 uses X-ray and optical data in an attempt to identify the best physical model for this source. We present our conclusions in § 5.

2. THE *ASCA* OBSERVATION

EXO 055620−3820.2 was observed by *ASCA* over the period 1995 March 23–24 with an on-source time ∼45 ks. As described in Tanaka, Inoue, & Holt (1994), *ASCA* has four identical, coaligned telescopes, two with solid state imaging spectrometers (SISs; Burke et al. 1991) and two gas imaging spectrometers (GIs; Ohashi et al. 1991) in the focal plane.

EXO 055620−3820.2 was observed with the SISs in two-CCD mode, with data accumulated in both FAINT and BRIGHT telemetry modes. As EXO 055620−3820.2 has a relatively low count rate in the SIS, the superior resolution available in FAINT mode could not be utilized. Therefore the FAINT and BRIGHT mode data were combined for the analysis presented here. Data were rejected by removing "hot" and "flickering" pixels in the SISs, by removing data accumulated during passages through the South Atlantic Anomaly, by imposing a minimum geomagnetic rigidity of 6 GeV c^{-1} (SIS) and 7 GeV c^{-1} (GIS), by removing data accumulated when the angle from the Earth's limb was less than 20° during orbit day and less than 5° during orbit night and by restricting SIS data to event grades 0, 2, 3, and 4. After these initial criteria had been applied, a light curve was constructed of the data from each instrument, and time periods of data dropout or spikes due to high background were removed manually. Application of these screening criteria gave a mean effective exposure time of ∼40 ks in all instruments.

Images were extracted from the screened and cleaned data from all instruments, and region descriptors defined for the extraction of light curves and spectra. For the two SIS instruments, we used a 3′ circle centered on EXO 055620−3820.2 , with the background taken at the edge of the same CCD chip. For the two GIS instruments, we used a circular extraction cell of 6′ radius centered on EXO 055620−3820.2 , with the background taken in a nearby source-free region.

The *ASCA* light curves reveal only low-amplitude flux variability (<20%), and, as the source was steady across more than 80% of the observation, with no evidence for any spectral variability, we consider only the mean spectrum in this paper.

3. SPECTRAL ANALYSIS

Data from both pairs of SIS and GIS instruments were analyzed together, but with the normalization of each dataset allowed to vary relative to the others (since there are small discrepancies in the absolute flux calibrations of the detectors).

A power-law model [$N(E)dE \propto E^{-\Gamma}dE$, where $N(E)$ is the photon flux density at energy E], corrected for photoelectric absorption (parameterized by an effective hydrogen column density $N_{\rm H}$, assuming the cross sections and abundances given by Morrison & McCammon 1983) does not provide an acceptable fit to the data ($\chi^2 = 1515$ for 1217 degrees of freedom [dof], leaving broad unmodeled structure in the data-minus-model residuals (Fig. 1). Such structure suggests

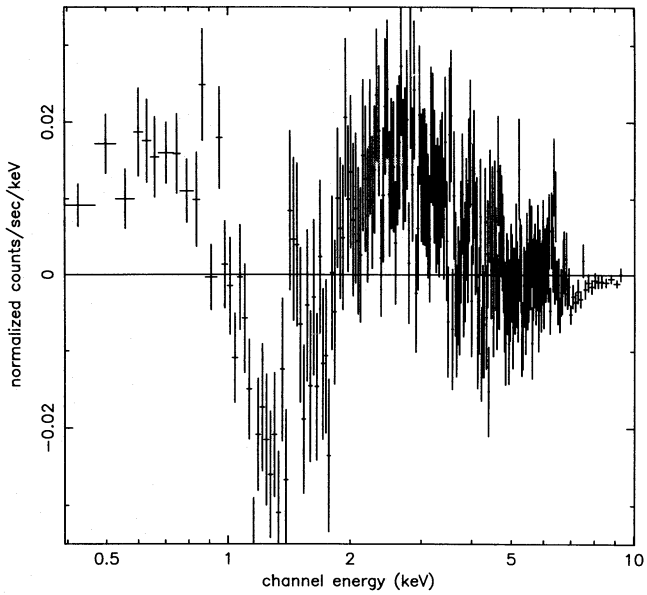

FIG. 1.—The data-minus-model residuals to a simple absorbed power-law model. All four *ASCA* instruments were fit, but only SIS0 data are shown here for clarity. Error bars of 1 σ are shown.

the need for a different/additional continuum component and/or complex absorber. In fact, we find several models below which adequately describe the X-ray spectrum. We describe each of these in turn, and then discuss them in the light of observations at other wavelengths in § 4. The observed 2–10 keV flux of the source was $F_{2-10} \simeq 2 \times 10^{-11}$ ergs cm^{-2} s^{-1}.

3.1. *The Iron-K-shell Regime*

Examining first the spectrum above 3 keV we find evidence (at >99% confidence) for an iron K-shell emission line. Modeling the 3–10 keV spectrum as a power-law continuum and a Gaussian emission line ($N(E) \propto 1/\sigma_z^l \exp[(E-E_z^l)^2/2\sigma_z^{l\,2}]$, where E_z^l is the line energy in the rest frame of the source and σ_z^l is its width) yields $\Gamma \sim 1.8$. As we will discuss later, complex model fits to the full 0.4–10 keV spectrum of this source show an underlying photon index of $\Gamma = 1.82^{+0.06}_{-0.07}$ (uncertainties are quoted at 90% confidence throughout). Thus, in this section we constrained Γ to the 90% confidence range (1.75–1.88) and examined the details of the iron line.

Assuming a narrow line (fixing σ_z^l at 0.0 keV), we obtain an acceptable fit for a line at $E_z^l \simeq 6.55$ keV with an equivalent width of 107^{+141}_{-42} eV (Table 1, model A). Allowing the width of the line to be free (Table 1, model B) yields a rest-frame energy $E_z^l \simeq 6.26$ keV, a width of $\sigma_z^l \simeq 0.47$ keV, and a much larger equivalent width of 277^{+154}_{-109} eV. The reduction of 19 in the χ^2 statistic, for one additional free parameter, indicates that the line is broad (at >99% confidence), which is confirmed by the formal constraints on σ_z^l when allowed to vary. The line energy is consistent with 6.4 keV, and hence with emission from neutral iron.

The data were also fitted with an emission-line profile of the form expected from the inner regions of a relativistic accretion disk. Such a profile has been suggested in NGC 3227 (George, Nandra, & Fabian 1990), and recently confirmed in MCG−6-30-15 (Tanaka et al. 1995). We use the parameterization described in Fabian et al. (1989) with the line emissivity varying as r^{-2} over the region $3r_{\rm S} < r <$

TABLE 1

SPECTRAL RESULTS FOR THE *ASCA* OBSERVATION OF EXO 055620−3820.2 PERFORMED 1995 MAR 23–24

Model	Model Expressions and Best-fitting Parameters[a]	Notes[b]	χ^2/dof
	Powerlaw + Line Fits to 3–10 keV Band		
A	PL + GL $E_z^l = 6.55^{+0.05}_{-0.55}$ keV	1, 2	621/631
B	PL + GL $E_z^l = 6.26^{+0.40}_{-0.22}$ keV $\sigma_z^l = 0.47^{+0.23}_{-0.19}$ keV	2	602/630
C	PL + DL $E_z^l = 6.40 < 6.51$ keV $i = 2^{+18}_{-2}$	2	617/630
	Full Covering by Ionized Material		
D	$A_0 \times A_z \times A_z^* \times$ (PL + GL) $N_{H,z} = 3.69^{+0.51}_{-0.37} \times 10^{21}$ cm^{-2} $N^*_{H,z} = 3.61^{+2.73}_{-2.18} \times 10^{22}$ cm^{-2} $\log_{10} U_x^* = -1.07^{+0.05}_{-0.05}$	2, 3, 4	1228/1216
	Partial Covering by Neutral Material		
E	$A_0 \times A_z \times \mathrm{PC}_z \times$ (PL + GL) $N_{H,z} = 0.0(<6.20) \times 10^{20}$ cm^{-2} $N^p_{H,z} = 2.57^{+0.14}_{-0.14} \times 10^{22}$ cm^{-2} $C_f^p = 96.6^{+0.5}_{-0.5}$% $\Gamma = 1.82^{+0.06}_{-0.07}$	3, 4	1177/1215
F	$A_0 \times \mathrm{A}_z \times \mathrm{PC}_z \times$ (PL + GL) $N_{H,z} = 1.50(<1.7) \times 10^{21}$ cm^{-2} $N^p_{H,z} = 2.51^{+0.14}_{-0.14} \times 10^{22}$ cm^{-2} $C_f^p = 95.0^{+0.5}_{-0.5}$% $\Gamma = 1.82^{+0.06}_{-0.07}$	3, 4	1208/1215
	Partial Covering by Ionized Material		
G	$A_0 \times A_z \times \mathrm{PC}_z^* \times$ (PL + GL) $N_{H,z} = 3.04^{+0.09}_{-0.07} \times 10^{21}$ cm^{-2} $C_f^p = 96.0\%$ (fixed) $N^{p*}_{H,z} = 3.11^{+1.33}_{-1.42} \times 10^{22}$ cm^{-2} $\log_{10} U_x^{p*} = -1.36^{+0.13}_{-0.16}$	2, 3, 4, 5	1235/1216

[a] The model functions and parameters are defined as follows: PL is the power-law continuum; GL The Gaussian emission line; DL the line emission from a relativistic disk, parameterized by its energy E_z^l and the angle i between the normal of the disk and the line of sight (see text); A the full-covering absorbing material, parameterized by an effective hydrogen column density N_H; PC the partial-covering absorbing material, parameterized by the covering fraction C_f^p of the absorption clouds, each with an effective hydrogen column density N_H. Quantities marked with a subscript z are either positioned at, or as measured in the rest frame of the source (with $z = 0.0344$); those marked with a subscript 0 are local ($z = 0$). Quantities marked with a superscript p refer to the component responsible for the partial covering, and those marked with an asterisk refer to the ionized material, with an ionization parameter U_x^* (as defined in the text).

[b] The following parameters were fixed in the lines indicated: (1) σ_z^l fixed at 0.0; Γ fixed at 1.8; (3) $N_{H,0}$ fixed at 3.35×10^{20} cm^{-2}; (4) E_z^l fixed at 6.26 keV, and σ_z^l at 0.47 keV; and (5) C_f^{p*} fixed at 96%.

$1000r_S$, where r_S is the Schwarzschild radius of the putative central black hole. We constrained the energy of the line to lie in the range 6.4–6.9 keV. The results of this fit (Table 1, model C) yielded a line with an equivalent width of 166 ± 47 eV and a rest-frame centroid energy $E_z^l = 6.40$ (<6.5) keV. The inclination angle of the disk was implied to be $i = 2^{-18}_{-2}{}^\circ$. Statistically we prefer a broad, Gaussian line over that expected from a relativistic disk.

The data are suggestive of an iron K-shell edge at ~ 7.1 keV, but the addition of such a component does not significantly improve the fit. We find an optical depth $\tau < 0.27$ for an edge fixed at a rest-frame energy of 7.1 keV.

3.2. *The Complex Broad-Band X-Ray Spectrum*

Next, the full 0.4–10 keV spectrum was analyzed, with iron K-shell line parameters fixed, in all ensuing models, at the best-fitting values derived assuming a broad, Gaussian line.

Below, we model the complex absorbing component in several different ways. First we present an investigation of

complete covering by ionized material. We continue by investigating alternative models, e.g., partial covering by neutral or ionized material. We use optical data to identify the most likely model for the absorber. We also discuss the possibility of an additional soft continuum component in this source. The fitting process is described below, while a discussion of the physical implications is postponed to § 4.

In the models involving ionized material, the data were fitted using model tables generated from the ION code (Netzer 1993, and see description below), and in those cases an underlying photon index of $\Gamma = 1.8$ was assumed, justified by the 3–10 keV fit (§ 3.1). (Experimentation with tables covering the 90% confidence range for Γ yielded similar results and conclusions.)

3.2.1. *Full Covering Ionized Absorption*

Evidence for the existence of ionized material in several AGNs (see § 1) suggests that such a component is made out of "small" clouds (i.e., gas condensations smaller than the central X-ray source; see Netzer 1993 and references therein), obscuring only a fraction of the power-law continuum source. This possibility, while physically plausible, is quite complex, since some of the emission from the ionized component may be observed without attenuation by the line-of-sight material (Netzer 1993; George et al. 1995).

The ionized models used here are described in Netzer (1993) and Netzer, Turner, & George (1994), but have been modified to include more extreme-ultraviolet lines and the most recent atomic data (Netzer 1996). Full radiative transfer, in line and continuum, is implemented in the models, and electron scattering and continuum fluorescence are included. The set of models used consists of thin spherical shells of constant hydrogen density $n_{\rm H} = 10^{11}$ cm^{-3} and variable column density. Solar composition is assumed throughout. We define an X-ray ionization parameter U_x^*, using the incident flux of X-ray photons over the 0.1–10 keV range. This definition is more meaningful for material ionized by X-rays, since it is less dependent on the softer Lyman continuum flux contributing to the lower ionization stages. Thus

$$U_x^* = \int_{\nu(0.1\,\rm keV)}^{\nu(10\,\rm keV)} \frac{L_\nu/h\nu}{4\pi r^2 n_{\rm H} c}\, d\nu\,, \qquad (1)$$

where r is the distance of the cloud from the ionizing source, $n_{\rm H}$ is the hydrogen density of the gas, L_ν is the monochromatic luminosity, and c is the speed of light. All models considered here have a typical AGN ultraviolet continuum with a blue bump, $\alpha_{\rm OX} \simeq 1.4$, and a photon index $\Gamma \simeq 1.8$ above 200 eV. For such a spectral shape, the ratio of the traditional ionization parameter $U(>1$ ryd) (e.g., Netzer 1990; defined over the full Lyman continuum) and the one used here is $U_x^*/U(>1\ \text{ryd}) = 0.004$.

Initially we attempted to model the absorption as a single-component ionized absorber, plus a neutral column fixed at the Galactic 21 cm value, $N_{\rm H,0} = 3.35 \times 10^{20}$ cm^{-2} (Elvis, Lockman, & Wilkes 1989). This model did not adequately describe the data, leaving a residual S-shape in the 1–2 keV regime. However, as shown by Fairall, McHardy, & Pye (1982), EXO 055620−3820.2 is an edge-on spiral galaxy with clear indications for an obscured nucleus. The observed Hα/Hβ line ratio is very large (18), far in excess of the distribution of this property in Seyfert 1 galaxies (e.g., Osterbrock 1977), and the optical continuum is much steeper than that normally seen in such AGNs (energy spectral index of about 3.4, compared to a typical slope of about 0.7 for Seyfert 1 galaxies). More recent observations of EXO 055620−3820.2 by Rafanelli (1985) give a lower value for the broad component Hα/Hβ line ratio (7.7), a somewhat shallower optical continuum slope (about 2.7 as estimated from his Fig. 1), but an extremely large ratio for the narrow components, Hα/Hβ = 23.6. These two observations are consistent, given the ambiguous separation of the broad and narrow components of the Balmer lines and the likely variability of the broad emission lines. However, even with the uncertainty on the shape of the intrinsic optical continuum, and the observed range of the intrinsic Hα/Hβ ratio in Seyfert 1 galaxies where large reddening is not suspected (Netzer 1990), the evidence for line-of-sight reddening in this source is compelling. This is further supported by the infrared and X-ray analysis of Ward et al. (1987), which shows the subclass of AGNs similar to EXO 055620−3820.2 to have large Hα/Hβ, steep optical-ultraviolet continua, and large L(6 keV)/Hα. Ward et al. (1987) argue that such objects (their "class B" AGNs) are all affected by line-of-sight reddening. Analysis of the X-ray spectra of some other reddened sources, such as MCG−6-30-15 (Reynolds et al. 1995), has not shown any requirement for a neutral screen associated with the dusty material which is causing the optical reddening. A geometry where the X-ray source is observed through a hole in the reddening material, or anomalous dust-to-gas ratios, may result in such a discrepancy. However, EXO 055620−3820.2 is a very highly reddened source compared to other Seyfert galaxies, and the neutral column associated with the optical reddening is proportionally high, making it easier to isolate in the X-ray analysis. This component was therefore included in the modeling as a full-covering absorbing screen of neutral material, with a column density $N_{{\rm H},z}$ at the redshift of the source. We assume this extra neutral absorbing material is located in the host galaxy, given the inclination of the host and the lack of such absorption in the nearby BL Lac EXO 055625−3838.6 (George & Turner 1996).

Given the optical line and continuum measurements above, we estimate the visual reddening of the continuum source, and the broad-line region (BLR) to be about $A_V = 2$ mag. The *minimum* (conservative) visual extinction consistent with the data is $A_V = 1$ mag, corresponding to a *minimum* full-covering column of neutral hydrogen of $N_{{\rm H},z} = 1.5 \times 10^{21}$ cm^{-2} assuming the Galactic dust-to-gas ratio.

We have considered two geometries for the ionized material: (*a*) a full shell with all emission and scattering components included, and (*b*) a very small covering factor of the ionized gas but a large cloud along the line of sight (i.e., the X-ray continuum is completely obscured, but the amount of ionized gas is very small compared to case *a*). As the data do not allow us to distinguish between cases *a* and *b*, we list only option *a* here, as model D in Table 1 (see also Fig. 2*a*).

Thus our first successful model assumes full obscuration by ionized material, with additional attenuation occurring from the full-covering screen of neutral material in the host galaxy, which turns out to be in good agreement with the observed reddening (Table 1, model D), plus the Galactic column due to material in our own Galaxy.

3.2.2. *Partial Covering by Neutral Material*

An alternative model, with the same number of free parameters as model D, is that of partial covering by

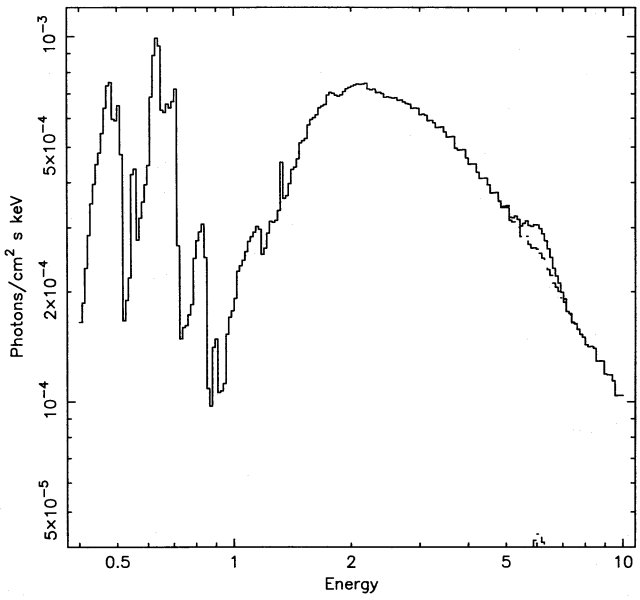

FIG. 2*a*

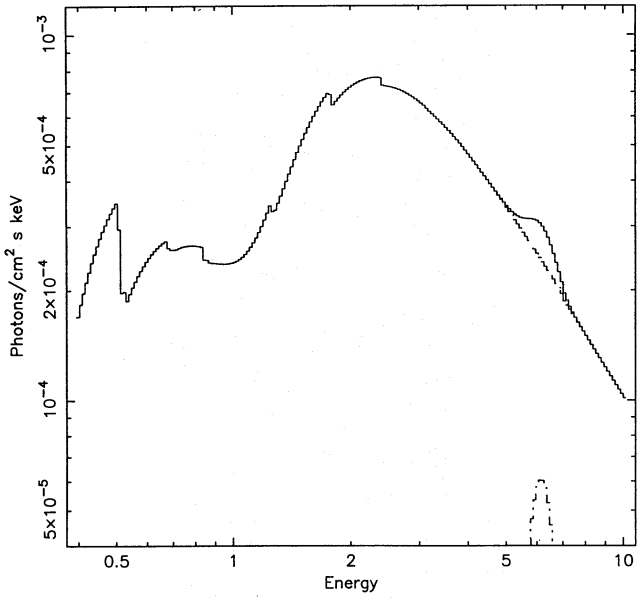

FIG. 2*b*

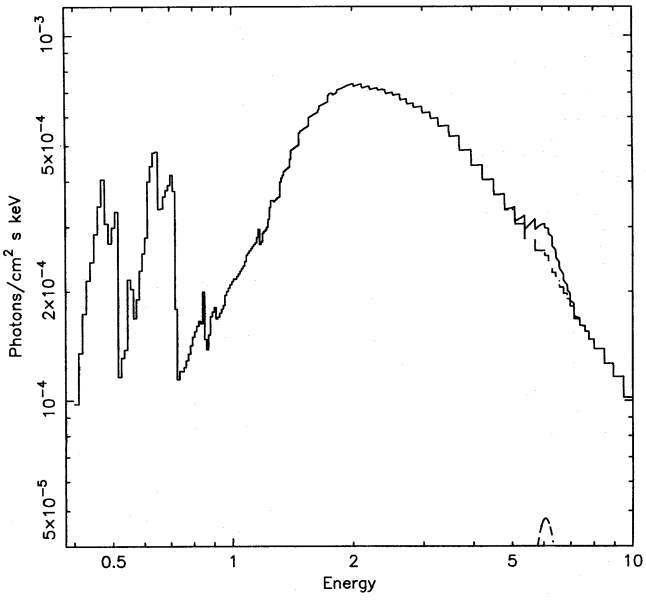

FIG. 2*c*

FIG. 2.—The best-fitting models to the EXO 055620−3820.2 data, as detailed in the text (§ 3.2) and tabulated in Table 1. (*a*) shows absorption by full-covering ionized material (model D), (*b*) absorption by neutral partial-covering material (model F), and (*c*) absorption by ionized partial-covering material (model G). The attenuation by the Galactic column and the best-fitting neutral full-covering screen is also included in each case.

neutral material. This model consists of an underlying power-law continuum (with a Gaussian line as described above due to iron K-shell emission) absorbed by three neutral components: a local (Galactic) screen fixed at the column derived from Galactic 21 cm measurements along the line of sight to the source and two components at the redshift of the source ($z = 0.0344$), a screen fully covering the source (associated with the optical reddening, as detailed above), and material partially covering the source. As this is an interactive XSPEC model, we simultaneously fit for the parameters of the absorber and the underlying photon index in this case.

The results of this analysis are shown in Table 1, model E. We find an acceptable fit ($\chi^2_\nu = 0.969$) for an underlying power law of $\Gamma = 1.82^{+0.06}_{-0.07}$, absorbed by a neutral column of $N^p_{\mathrm{H},z} \simeq 2.6 \times 10^{22}$ cm^{-2} covering $C^p_f \simeq 97\%$ of the source, while the full-covering screen goes to zero.

We repeated the fit with the full-covering screen constrained to lie above the minimum column of neutral hydrogen consistent with reddening measurements, $N_{\mathrm{H},z} = 1.5 \times 10^{21}$ cm^{-2}, as determined in § 3.2.1 above.

The best-fitting parameters of this model are shown in Table 1, model F, while the model is illustrated in Figure 2*b*. It can be seen that this model provides an adequate fit to the data with parameters very similar to those for model E. However, it should be noted that the column of the additional absorbing screen $N_{\mathrm{H},z}$ "pegs" at the lowest allowed value, and has a 1 σ upper limit of 1.7×10^{21} cm^{-2}. Furthermore, enforcement of the constraint on $N_{\mathrm{H},z}$ results in a *systematic excess* of counts over the model below $\simeq 1$ keV

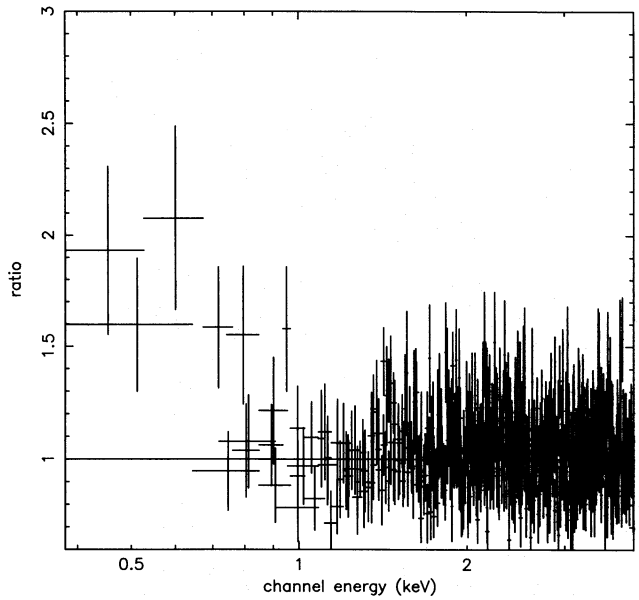

FIG. 3.—The ratio of the data to the neutral partial-covering model F. This illustrates the systematic excess of counts below ~1 keV, which is discussed extensively in § 4.3.3.

(Fig. 3). This soft component contributes $F_{0.4-1} \simeq 1.2 \times 10^{-13}$ ergs cm^{-2} s^{-1} ($\simeq$50% of the total) in the 0.4–1 keV band, implying an *observed* luminosity[4] $L^{\rm obs}_{0.4-1} \simeq 3.2 \times 10^{41}$ ergs s^{-1} in this band. We investigate this soft excess further in § 3.2.4; we postpone discussion of the absorber until § 4.

3.2.3. *Partial Covering by Ionized Material*

The overall success in fitting the observed spectrum with a model including partial covering of the central source, led us to consider cases where the partially covering screen is close to the central continuum source, and is therefore highly ionized. We assumed an underlying continuum slope $\Gamma = 1.8$ (as justified in § 3.1). Model D in § 3.2.1 deals with an ionized absorber fully covering the source ($C^p_f = 100\%$). An iterative fitting process was used to determine the minimum covering fraction consistent with the spectral curvature in the 2 keV regime, caused by absorption. These fits showed the minimum covering fraction consistent with the data to be $C^p_f = 96\%$. We pursue a detailed treatment of this model, and thus the two ionized absorber models presented in Table 1 (D and G) encompass the range of parameter space for the covering fraction appropriate for this source.

A Galactic screen of neutral material $N_{\rm H,0}$, was fixed at 3.35×10^{20} cm^{-2}, as before. We then fitted for the column density of the screen of neutral material at the source ($N_{{\rm H},z}$), the column density of the ionized gas covering 96% of the source ($N^{p*}_{{\rm H},z}$), and the X-ray ionization parameter (U^*_x). The results are given in Table 1, model G. The model is a good fit to the data; the model parameters are similar to those obtained for the full-covering case. The model is shown in Figure 2*c*. Despite the inclusion of emission from the ionized cloud, we again see an excess of soft emission, which we investigate further in § 3.2.4. We postpone discussion of the absorber until § 4.

3.2.4. *The Soft Excess*

We attempted to parameterize the low-energy excess (evident in the residuals to the partial-covering models described in § 3.2.2 and § 3.2.3) by a simple model in order to estimate its intrinsic luminosity. This requires some assumptions about the location and spectral form of the component. We hypothesize that the excess is emission from a hot plasma and parameterize it using standard Raymond and Smith models (leaving all other parameters fixed at the values in Table 1 model F or G). For the following locations our results are the following:

1. *Hot plasma behind the partial covering absorber.*—Here, the hypothetical soft component is located in the innermost part of the AGN, close to the power-law continuum source. The attenuation of the flux of this component is identical to that of the central continuum, i.e., absorption by the partial-covering material and the two complete neutral-gas screens. In the case of the neutral partial-covering model *F* inclusion of this component reduced the fit statistic by $\Delta\chi^2 = 23$ for a plasma of temperature $kT = 0.14^{+0.05}_{-0.06}$ keV. In this case the unabsorbed (intrinsic) luminosity of this component is $L^{\rm soft}_{0.4-1} = 3.1 \times 10^{43}$ ergs s^{-1}, which is $\simeq$57% of the total unabsorbed luminosity $L^{\rm tot}_{0.4-1}$, in the 0.4–1 keV band. In the case of the *ionized* partial-covering model G, its inclusion reduced the fit statistic by $\Delta\chi^2 = 6$ for a plasma of temperature $kT = 0.09^{+0.05}_{-0.06}$ keV. The implied intrinsic (unabsorbed) luminosity of the soft component in this case is $L^{\rm soft}_{0.4-1} = 3.5 \times 10^{43}$ ergs s^{-1}, i.e., 60% of $L^{\rm tot}_{0.4-1}$.

2. *Hot plasma between the partial-covering absorber and the full-covering absorber.*—The location of the soft component is farther away from the nucleus, and could correspond to the location of the narrow-line region (NLR). The soft component is only attenuated by the two neutral screens (and not by the additional factor of 20 due to the thick partial-covering component). In the case of the neutral partial-covering model *F*, its inclusion reduced the fit statistic by $\Delta\chi^2 = 18$ with a best-fitting plasma temperature of $kT = 0.11^{+0.04}_{-0.05}$ keV. Under this scenario $L^{\rm soft}_{0.4-1} = 1.3 \times 10^{42}$ ergs s^{-1} representing $\simeq$5% of $L^{\rm tot}_{0.4-1}$. In the case of the ionized partial-covering model G, its inclusion reduced the fit statistic by $\Delta\chi^2 = 17$ for a plasma temperature of $kT = 0.14^{+0.04}_{-0.05}$ keV. This gives an unabsorbed $L^{\rm soft}_{0.4-1} = 3.61 \times 10^{42}$ ergs s^{-1} (6% of $L^{\rm tot}_{0.4-1}$ keV.

3. *Hot plasma outside the full-covering redshifted neutral screen*—In this case the location of the soft component is far from the nucleus and may correspond to the outskirts of the host galaxy. Inclusion of a soft spectral component in this way reduced the fit statistic by $\Delta\chi^2 = 19$. As this case involves an origin outside of the X-ray absorber, the results are the same for the neutral and ionized cases. The best-fitting plasma temperature is $kT = 0.14^{+0.05}_{-0.06}$ keV, which suggests an unabsorbed $L^{\rm soft}_{0.4-1} = 3.9 \times 10^{41}$ ergs s^{-1}, $\simeq$2% of $L^{\rm tot}_{0.4-1}$.

We stress that the signal-to-noise ratio in this part of the spectrum is rather low and the energy range very small. Thus, the fit results should not be overinterpreted. We postpone discussion of these findings until § 4.

3.2.5. *Additional Models*

We have experimented with various other models, trying to cover more of the available parameter space. In particular, we have verified that the spectrum is well described by two different continuum components (e.g., a power-law and a hot plasma), if each component is allowed to pass through independent (different) absorbing material. However, we do

[4] $H_0 = 70$ km s^{-1} Mpc^{-1}, $q_0 = 0.5$ assumed throughout.

not show these fits, since the quality of the data warrants no meaningful interpretation of models with such a large number of free parameters. While we cannot rule out such ad hoc models, we consider them the least compelling explanation for the data.

4. DISCUSSION

4.1. *The Iron K-Shell Regime*

EXO 055620−3820.2 shows clear evidence for an iron K-shell emission line. The equivalent width of the line is ∼100 or ∼300 eV, depending respectively on whether a narrow or broad line is assumed. The former value is easily consistent with predictions based on reflection from an optically thick accretion disk when observed close to face-on (George & Fabian 1991). The latter value exceeds the maximum obtainable from such disk, unless the iron abundance exceeds that given in Morrison & McCammon (1983) by a factor of ∼2 (George & Fabian 1991; Reynolds, Fabian, & Inoue 1995), and/or the primary continuum source preferentially emits toward the disk. Both of these possibilities are feasible. The maximum amount of iron K-shell line emission expected from the line-of-sight absorbing material is ∼25 eV for Table 1 model G and somewhat smaller for models F and D. Constraints on the line width (σ_z^l) of EXO 055620−3820.2 suggest that the line may be intrinsically broad as has been found to be the case for several AGNs (e.g., Mushotzky et al. 1995; Tanaka et al. 1995). In that case, the line energy is consistent with emission from neutral iron. We find $\sigma_z^l \sim 0.5$ keV, corresponding to a FWHM for the line of 31,000–77,000 km s^{-1}. We find the line to be consistent with, but not required to have, the distinctive asymmetric line profile expected from an accretion disk (e.g., Fabian et al. 1989). However, we caution that unresolved spectral complexity in the iron K-shell regime can give rise to misleading results, and even mimic a broad line.

4.2. *Full-Covering Ionized Absorption*

This model (model D) seems to be the best from the point of view of a minimal number of components, the low energy fit to the data, and the consistency with the neutral-screen reddening.

Our spectral analysis suggests that a single absorbed power-law continuum, with a slope of $\Gamma = 1.8$, explains both the iron K-shell regime as well as the low energy (0.4–1.0 keV) *ASCA* data. The column density is only slightly larger than that deduced from partial-covering models but the ionization parameter is larger by a factor of 2. This forces the neutral screen to a column density corresponding to $A_V \simeq 2$ mag close to that independently determined from optical line and continuum measurements (§ 3.2.1). The ionized screen is so highly ionized that dust is not likely to form or survive at this location and the gas is completely transparent at energies below 0.3 keV.

As explained in § 3, we are unable to distinguish between pure absorption by the ionized gas and a case where emission is also important. This is partly a result of the low signal-to-noise ratio at low energies and partly because the emission features predicted are relatively weak. However, a visual inspection suggests a similarity between some of the observed features and the calculated emission lines (Fig. 4). We have therefore looked for the strongest emission features predicted by the model. These are O VII 568 eV

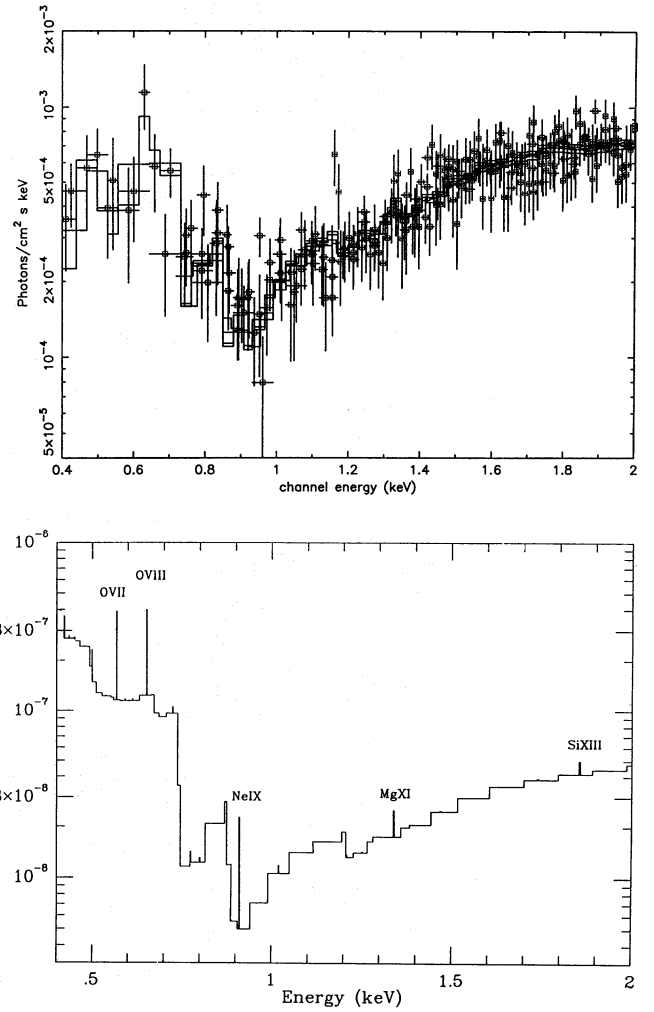

FIG. 4.—*Top panel*: The best-fit model of a power law attenuated by full-covering ionized absorption (model D). The model includes self-consistent line emission and is shown with the unfolded *ASCA* data. *Bottom panel*: The ionized-absorber model D at the resolution calculated for the model-fitting tables.

(equivalent width, EW, of 17 eV); O VIII 653 eV (EW = 19 eV), Ne IX 911 eV (EW = 41 eV), and Mg XI 1.34 keV (EW = 6 eV). All numbers refer to the *observed* equivalent width, that is, relative to the local observed continuum. The Ne IX 911 eV line is, in fact, intrinsically the weakest, but is observed against a highly absorbed part of the continuum, and hence has the largest equivalent width. (For a more complete discussion of these effects and line intensities see Netzer 1996). We also note that the presence of a Ne IX 911 eV line of twice the predicted strength might explain why we do not observe as sharp an absorption feature as predicted by the model (see Figure 3). This is not unreasonable in view of the possible complex geometry near such sources.

4.3. *Partial-Covering Models*

Our analysis of the X-ray spectrum of EXO 055620−3820.2 indicates that partial covering by small clouds (either neutral or ionized, with a large covering factor) can explain the hard X-ray continuum. However, we find such models reveal evidence for significant excess emission below ∼1 keV.

Partial covering of the AGNs X-ray continuum source, was first suggested as an explanation of the soft excess

observed in NGC 4151 (Holt et al. 1980). Partial-covering models have been investigated in some detail for NGC 4151 (e.g., Yaqoob et al. 1993; Weaver et al. 1994a) and other sources (Bond & Matsuoka 1993; Maisack et al. 1992), and may be applicable to many AGNs. The most recent analysis of NGC 4151 by Weaver et al. (1994a) discusses a "duel absorber," where 40% of the source is covered by a column 6×10^{22} cm^{-2} and the other 60% by 2–3 $\times$ 10^{23} cm^{-2}. In the case of NGC 4151, however, the columns involved are an order of magnitude larger than those considered here.

4.3.1. *Partial Covering by Neutral Material*

Considering first partial covering by neutral material (models E and F), such a component must be far from the source to maintain the very low level of ionization. The large partial-covering column of neutral material (2.5×10^{22} cm^{-2}) implied by our analysis is likely to be associated with dust which, given a Galactic dust-to-gas ratio, is completely opaque at optical and ultraviolet wavelengths. Thus the optical continuum passing through this shell must be attenuated by a factor of approximately 20 (the covering fraction is 95%), compared with the flux above 3 keV (which is passing through a transparent medium). Thus the intrinsic optical flux must be considerably higher than that observed, and the intrinsic α_{ox} must be steeper by $\Delta\alpha_{ox} = 0.5$ than that observed. We used the Rafanelli (1985) optical observations at 5000 Å (which are already affected by reddening), to calculate the 2500 Å flux, and this, together with our 2 keV flux measurement, was used to deduce the intrinsic α_{ox} for the source. (While the 2 keV flux is not completely free of absorption effects, this is the most useful number to use for comparison with other objects.) We do not know the exact amount of visual reddening; therefore, we considered two possibilities.

Assuming $A_V = 2$ mag and an unreddened energy slope of 0.7 between 5000 and 2500 Å, then correcting for the reddening by the full-covering screen we get $\alpha_{ox} = 1.49$. As explained earlier, an additional correction to the 2500 Å point due to the presence of the partial-covering neutral material results in an implied intrinsic $\alpha_{ox} = 1.99$. Repeating the same procedure, but assuming $A_V = 1$ mag, we get $\alpha_{ox} = 1.33$ with no correction for the neutral partial covering, and an implied intrinsic α_{ox} of 1.83 with that correction.

The two values of deduced intrinsic α_{ox} (above) are larger than those observed in most Seyfert 1 galaxies, where a typical range in this property is about 1.1–1.5 (Kriss & Canizares 1985; Stocke et al. 1991). Our values are, in fact, in the range found for radio-quiet quasars. On the other hand, correcting only for the full-covering neutral screen yields $\alpha_{ox} = 1.33$–1.49, in perfect agreement with that observed for unreddened AGNs (e.g., the class A″ AGN of Ward et al. 1987). We note that values of α_{ox} derived here are subject to uncertainties in the shape of the intrinsic optical-ultraviolet continuum (used to estimate the 2500 Å flux) and to optical and X-ray variability.

A similar conclusion is obtained from consideration of the optical luminosity of the source. Correcting for up to 2 magnitudes of visual extinction implies that EXO 055620−3820.2 is intrinsically somewhat more luminous than a typical Seyfert 1 galaxy, such as NGC 5548 (see Table 4 of Ward et al. 1987). The additional attenuation factor of 20, implied by an opaque partial-covering screen, suggests that it is intrinsically almost as luminous as 3C 273. Thus, under the neutral partial-covering scenario, the implication is that this galaxy hosts one of the most luminous quasars, at a distance corresponding to $z = 0.0344$. We consider this to be very unlikely, especially as our ionized-absorption models infer more typical intrinsic X-ray and optical luminosities for this source.

4.3.2. *Partial Covering by Ionized Material*

The problem of a large implied optical flux does not exist for the ionized partial-covering model. In this case, the ionization level of the material indicates, for the assumed large gas density, a location in the innermost part of the AGN. Gas clouds in this location are likely to be smaller than the X-ray source size (e.g., the BLR clouds), and conditions are such that dust cannot form (e.g., Netzer & Laor 1993). The possibility of high-ionization, low-density material, much further from the center, is more difficult to analyze, but conditions in such gas are also not favorable for dust formation. The ionized-partial-covering model predicts an intrinsic α_{ox} which is inside the overall Seyfert 1 distribution of this property, as, in this case the reddening is only by the complete-coverage neutral screen, which exists much further from the nucleus. Thus there is no need to assume an extreme intrinsic luminosity for this source, and we conclude that optical data favor the ionized absorption models for this source.

4.3.3. *The Nature of the Soft Excess*

Both partial-covering models discussed in the preceeding subsections leave a large residual soft excess below 1 keV. (Interestingly, the soft excess contributes about 50% of the observed flux below 1 keV, the same fractional contribution as the extended component in NGC 4151; see Weaver et al. 1994.) The implied luminosity in this component is obviously highly dependent upon its location relative to our three absorbing components. Since the luminosities are similar in the neutral and ionized cases, we combine the discussion of the two.

1. *Hot plasma behind the partial-covering absorber.*—Here the soft component originates in the innermost part of the AGN, close to the power-law continuum source. The implied luminosity is $L^{\rm soft}_{0.4-1} = 3$–4×10^{43} ergs s^{-1} which is $\sim$60% of $L^{\rm tot}_{0.4-1}$, and $\sim$33% of $L^{\rm tot}_{0.4-1}$. A *possible* origin for this soft emisson is the inner regions of the putative accretion disk, either arising as a result of X-ray emission from the inner regions of a high-temperature disk (e.g., Laor 1990), or from reflection of the central X-ray flux by the disk atmosphere (e.g., Zycki et al. 1994). We note that in both cases, the luminosity in this soft component is larger than that obtainable by current models.

2. *Hot plasma between the partial-covering absorber and the full-covering absorber.*—In the second scenario, the soft component originates further away from the nucleus, between the partial-covering X-ray absorber, and the full-covering (reddening) screen. This origin may correspond to hot gas in pressure equilibrium with the NLR. Such a component has been discussed by Marshall et al. (1993) in the case of NGC 1068, and by Krolik & Kriss (1995) in the general case. In NGC 1068 the temperature of the gas is $\sim 10^6$ K, but the integrated X-ray luminosity is much smaller than the measured luminosity in EXO 055620−3820.2 ($L^{\rm soft}_{0.4-1} \sim 6\%$ of $L^{\rm tot}_{0.4-1}$ § 3.2.2 and § 3.2.3). Weaver et al. (1994) proposed that the temperature expected from shock heating of outflowing narrow line

keV. We suggest that the required X-ray luminosity in EXO 055620−3820.2 is too large to be consistent with these models.

3. *Hot plasma outside the full-covering redshifted neutral screen.*—As stated earlier, this location may correspond to the outskirts of the host galaxy. Normal galaxies have extended soft X-ray emission, which is the sum of the contributions from sources such as accreting binaries, supernova remnants, and the hot interstellar medium and halo of the galaxy. *Einstein* observations of spiral galaxies found 0.2–3.5 keV luminosities in the range $10^{38} \lesssim L_{0.2-3.5}^{\rm soft} \lesssim 10^{41}$ ergs s^{-1} (Fabian 1981; Long & Van Speybroeck 1983; Fabbiano 1984, 1986, 1989), although thermal emission from the interstellar medium, heated by supernovae, could give rise to $L_{0.2-3.5}^{\rm soft} \sim 10^{42}$ ergs s^{-1} (see Fabbiano 1989). EXO 055620−3820.2 lies at the high end of this distribution with $L_{0.2-3.5}^{\rm soft} = 8.8 \times 10^{41}$ ergs s^{-1}.

The intrinsic luminosity of the soft excess in EXO 055620−3820.2 is $L_{0.2-2}^{\rm soft} = 1.2 \times 10^{42}$ ergs s^{-1}, a factor of 4 higher than that reported for the soft extended component in NGC 4151 (Morse et al. 1995), and slightly higher (factor of ∼2) than the most luminous extended components noted by Weaver et al. (1995) for other AGNs. However, for NGC 4151 the absorption-corrected luminosity ranges from $L_{2-10} \sim 3$–20×10^{42} ergs^{-1}, while EXO 055620−3820.2 has $L_{2-10} \sim 6 \times 10^{43}$ ergs^{-1}. As the nucleus of EXO 055620−3820.2 is more than a factor of 4 times more luminous than that of NGC 4151, any nuclear-driven excess, might be expected to result in a more luminous soft emission in EXO 055620−3820.2.

If the soft component originates in the outskirts of the host galaxy then it must be constant in flux on a timescale of years, hence the same component should be observable in previous soft X-ray observations of this source. EXO 055620−3820.2 was observed by the *ROSAT* PSPC on 1993 Sept 25 for ∼13 ks, and we have examined those data in the light of the *ASCA* results. The PSPC spectrum shows the same strong signature of complex absorption observed in the *ASCA* data, while the source has an integrated 0.1–2 keV flux ∼35% of that observed at the *ASCA* epoch. The PSPC data confirm the softening of the spectrum to lower energies, and are consistent with the presence of a soft component at the flux level inferred by the *ASCA* data, although we note that the PSPC data prefer a plasma temperature $\sim 0.23^{+0.05}_{-0.04}$ keV. As the PSPC and *ASCA* data are from two different epochs, we do not consider joint *ASCA* and *ROSAT* fitting any further.

5. SUMMARY AND CONCLUSIONS

The first uncontaminated hard X-ray spectrum of the Seyfert 1 galaxy EXO 055620−3820.2 shows complex structure below ∼2 keV, indicative of attenuation either by an ionized absorber fully or partially covering the X-ray source, or a neutral absorber partially covering the source. While the X-ray data alone do not allow us to distinguish between these models, consideration of the optical properties of the source suggests that partial-covering by neutral material is unlikely, as the implied intrinsic optical flux would be unusually large (§ 4.3.1). We find a good fit to the X-ray data, and consistency with the observed optical properties of the source, with either 96% of the source covered by a column of 3.1×10^{22} cm^{-2} of ionization state $\log_{10} U_x^* = -1.36$, or full covering by a column of 3.6×10^{22} cm^{-2} with $\log_{10} U_x^* = -1.07$. In the case of the partial-covering model, we find a residual soft excess, whose origin seems most likely to be either from the outskirts of the host galaxy, or from hot gas in pressure equilibrium with the NLR. The full-covering ionized absorber model is the preferred explanation for EXO 055620−3820.2, from the point of view of its simplicity.

In addition to the complex absorber, we find evidence for a full-covering screen of neutral material, which is consistent with the column implied by optical reddening. We also detect an iron K-shell emission line, which appears to be significantly broad and whose equivalent width of ∼300 eV exceeds that predicted to arise in the absorbing material, as for many other Seyfert spectra recently reported. We find a FWHM for the line of 31,000–77,000 km s^{-1}.

We thank the anonymous referee for comments which greatly improved the final paper. We also thank Paul Nandra, Richard Mushotzky, Tim Kallman, and Tahir Yaqoob for useful discussions. We acknowledge the financial support of the Universities Space Research Association (I. M. G., T. J. T.) and NASA grant NAS5-32490 (H. N.). The analysis was performed using XSELECT (version 1.3) and XSPEC (version 8.5). This research made use of the SIMBAD database, operated at CDS, Strasbourg, France; the NASA/IPAC Extragalactic Database (NED) operated by the Jet Propulsion Laboratory, Caltech, under contract with NASA; and of data obtained through the HEASARC on-line service, provided by NASA/GSFC.

REFERENCES

Bond, I. A., & Matsuoka, M. 1993, MNRAS, 265, 619
Burke et al. 1991, IEEE Trans. Electron Devices, 38, 1069
Elvis, M., Lockman, F. J., & Wilkes, B. J. 1989, AJ, 97, 777
Fabbiano, G. 1984, X-Ray Astronomy '84, ed. M. Oda & R. Giacconi (Tokyo: Inst. Space Astronautical Sci.), 333
———. 1986, PASP, 98, 525
———. 1989, ARA&A, 27, 87
Fabian, A. C. 1981, in The Structure and Evolution of Normal Galaxies, ed. S. M. Fall & D. Lynden-Bell (Cambridge: Cambridge Univ. Press), 181
Fabian, A. C., Rees, M. J., Stella, L., & White, N. E. 1989, MNRAS, 238, 729
Fabian, A. C., et al. 1994, PASJ, 46, L59
Fairall, A. P., McHardy, I. M., Pye, J. P. 1982, MNRAS, 198, 13P
Ferland, G. J., & Rees, M. J. 1988, ApJ, 332, 141
Fiore, F., Elvis, M., Mathur, S., Wilkes, B., & McDowell, J. C. 1993, ApJ, 415, 129
Fiore, F., Perola, G. C., & Ramano, M. 1990, MNRAS, 243, 522
George, I. M., & Fabian, A. C. 1991, MNRAS, 249, 352
George, I. M., & Turner, T. J. 1996, ApJ, in press
George, I. M., Nandra, K., & Fabian, A. C. 1990, MNRAS, 242, 352
George, I. M., Turner, T. J., & Netzer, H. 1995, ApJ, 438, L67
Giommi, P., Neuermann, K., Barr, P., Schwope, A., Taglaferri, G., & Thomas, H. C. 1989 MNRAS, 236, 375
Halpern, J. 1984, ApJ, 281, 90
Holt, S. S., et al. 1980, ApJ, 241, L13
Kriss, G., & Canizares, C. 1985, ApJ, 297, 177
Krolik, J., & Kallman, T. 1984, ApJ, 286, 355
Krolik, J., & Kriss, G. 1995, ApJ, 447, 512
Laor, A. 1990, MNRAS, 246, 369
Long, K. S., & Van Speybroeck, L. P. 1983, in Accretion Driven X-Ray Sources, ed. W. Lewin & E. P. J. van den Heuvel (Cambridge: Cambridge Press), 117
Mathur, S., Wilkes, B., Elvis, M., & Fiore, F. 1994, ApJ, 434, 493
Maisack, M., et al. 1992, Astron. Astrophys. Trans., 262, 433
Marshall et al. 1993, ApJ, 405, 168
Morrison, R., & McCammon, D. 1983, ApJ, 270, 119
Morse, J. A., Wilson, A. S., & Elvis, M. 1995, ApJ, 439, 121

Mushotzky, R. F., Fabain, A. C., Iwasawa, K., Kunieda, H., Matsuoka, M., Nandra, K., & Tanaka, Y. 1995, MNRAS, 272, L9
Nandra, K., & Pounds, K. 1994, MNRAS, 268, 405
———. 1992, Nature, 359, 215
Netzer, H. 1990, in Active Galactic Nuclei (Berlin: Springer), 57
———. 1993, ApJ, 411, 594
———. 1996, ApJ, (in prep)
Netzer, H., & Laor, A. 1993, ApJ, 404, L51
Netzer, H., Turner, T. J., & George, I. M. 1994, ApJ, 435, 106
Ohashi, T., Makishima, K., Ishida, M., Tsuru, T., Tashiro, M., Mihara, T., Kohmura, Y., & Inoue, H. 1991, Proc. SPIE, 1549, 9
Osterbrock, D. E. 1977, ApJ, 215, 733
H., Stewart, G. C., & Pounds, K. A. 1990, MNRAS, 242, 177
Piccinotti, G., et al. 1982, ApJ, 253, 485
Rafanelli, P. 1985, Astron. Astrophys. Trans., 146, 17
Reynolds, C. S., & Fabian, A. C. 1995, MNRAS, 273, 1167
Reynolds, C. S., Fabian, A. C., & Inoue, H. 1995b, MNRAS, in press
Reynolds, C. S., Fabian, A. C., Nandra, K., Inoue, H., Kunieda, H., & Iwasawa, K. 1995a, MNRAS, in press
Stocke, J. T., Morris, S., Gioia, I. M., Maccacaro, T., Schild, R., Wolter, A., Fleming, T., & Henry, P. 1991, ApJS, 76, 813
Tanaka, Y., Inoue, H., & Holt, S. S. 1994, PASJ, 46, L37
Tanaka, Y., et al. 1995, Nature, 375, 659
Turner, T. J., Nandra, K., George, I. M., Fabian, A. C., & Pounds, K. A. 1993, ApJ, 419, 127
Ward, M., Elvis, M., Fabiano, G., Carleton, N. P., Willner, S. P., & Lawrence, A. 1987, ApJ, 315, 74
Weaver et al. 1994, ApJ, 423, 621
Weaver, K., Mushotzky, R. F., Serlemitsos, P. J., Wilson, A. S., Elvis, M., & Briel, U. 1995, ApJ, 442, 597
Weaver, K., Yaqoob, T., Holt, S. S., Mushotzky, R. F., Matsuoka, M., & Yamauchi, M. 1994a, ApJ, 436, L27
Yaqoob, T. 1990. Ph.D. thesis, Univ. Leicester, UK
Yaqoob, T., & Warwick, R. S. 1991, MNRAS, 248, 773
Yaqoob, T., Warwick, R. S., Makino, F., Otani, Y., & Sokoloski, J. 1993, MNRAS, 262, 435
Zycki, P. T., Krolik, J. H., Zdziarski, A. A., & Kallman, T. R. 1994, ApJ, 437, 597